First-principles thermodynamics and defect kinetics guidelines for engineering a tailored RRAM device

Article *in* Journal of Applied Physics · June 2016

DOI: 10.1063/1.4953673

9 authors, including:

Sergiu Clima
IMEC International
78 PUBLICATIONS **878** CITATIONS
SEE PROFILE

Yang Yin Chen
SanDisk
69 PUBLICATIONS **771** CITATIONS
SEE PROFILE

L. Goux
IMEC International
200 PUBLICATIONS **1,661** CITATIONS
SEE PROFILE

Bogdan Govoreanu
IMEC International
131 PUBLICATIONS **1,743** CITATIONS
SEE PROFILE

AIP | Journal of Applied Physics

First-principles thermodynamics and defect kinetics guidelines for engineering a tailored RRAM device

Sergiu Clima, Yang Yin Chen, Chao Yang Chen, Ludovic Goux, Bogdan Govoreanu, Robin Degraeve, Andrea Fantini, Malgorzata Jurczak, and Geoffrey Pourtois

Citation: Journal of Applied Physics **119**, 225107 (2016); doi: 10.1063/1.4953673
View online: http://dx.doi.org/10.1063/1.4953673
View Table of Contents: http://scitation.aip.org/content/aip/journal/jap/119/22?ver=pdfcov
Published by the AIP Publishing

JOURNAL OF APPLIED PHYSICS **119**, 225107 (2016)

First-principles thermodynamics and defect kinetics guidelines for engineering a tailored RRAM device

Sergiu Clima,[1,a)] Yang Yin Chen,[1] Chao Yang Chen,[1,2] Ludovic Goux,[1] Bogdan Govoreanu,[1] Robin Degraeve,[1] Andrea Fantini,[1] Malgorzata Jurczak,[1] and Geoffrey Pourtois[1,3]
[1]*imec, Kapeldreef 75, 3001 Leuven, Belgium*
[2]*Katholieke Universiteit Leuven, 3001 Leuven, Belgium*
[3]*PLASMANT, University of Antwerp, 2610 Antwerpen, Belgium*

(Received 5 February 2016; accepted 29 May 2016; published online 10 June 2016)

Resistive Random Access Memories are among the most promising candidates for the next generation of non-volatile memory. Transition metal oxides such as HfOx and TaOx attracted a lot of attention due to their CMOS compatibility. Furthermore, these materials do not require the inclusion of extrinsic conducting defects since their operation is based on intrinsic ones (oxygen vacancies). Using Density Functional Theory, we evaluated the thermodynamics of the defects formation and the kinetics of diffusion of the conducting species active in transition metal oxide RRAM materials. The gained insights based on the thermodynamics in the Top Electrode, Insulating Matrix and Bottom Electrode and at the interfaces are used to design a proper defect reservoir, which is needed for a low-energy reliable switching device. The defect reservoir has also a direct impact on the retention of the Low Resistance State due to the resulting thermodynamic driving forces. The kinetics of the diffusing conducting defects in the Insulating Matrix determine the switching dynamics and resistance retention. The interface at the Bottom Electrode has a significant impact on the low-current operation and long endurance of the memory cell. Our first-principles findings are confirmed by experimental measurements on fabricated RRAM devices. *Published by AIP Publishing.* [http://dx.doi.org/10.1063/1.4953673]

I. INTRODUCTION

The economics behind mass-produced memory electronic nano-devices dictate that their density/performance has to double every ~2 years to be cost-effective. The present Flash memory technology is close to the physical limits of size downscaling. Therefore, a replacement technology is needed to enforce the established trends. Electrically switchable resistance change memories (Resistive Random Access Memories—RRAM) are currently assessed to establish whether they can be a worthy replacement.[1,2]

The TaO_x, HfO_x materials used in Oxide-based RRAMs (OxRAM) are CMOS-compatible,[3] they were shown to scale down to 10 nm,[4] but for successful large array implementation a low-current reliable operation (<10 uA) is required. While the sub-10 uA operation is not a problem "per se," having most of the devices in the array within a narrowly distributed resistance range (non-overlapping high resistive state (HRS)/low resistive state (LRS) of 3–4σ), high cyclability and stable in time has, however, proved to be challenging for these type of materials.[5] In order to provide electrical engineers with guidance on how to improve the different device properties, we analyze in the present work the different RRAM functional part materials, their properties, and put them into prospective in terms of device performances and how these influence each other.

The RRAM working principles are generally well-established,[6–14] they differ for different classes of materials. There are systems that show resistance change in the bulk of the materials like VO_2/NbO_2[15] or induced by the moving front of defects like in anatase TiO_2.[16] The OxRAM devices that we investigate in the present work usually show a resistance switch mechanism using a 1D filament made of oxygen vacancies and operated in a bipolar fashion (Figure 1(a)).[7,9,17,18] Usually, the RRAM devices need a preparatory step to have well-behaved devices, called FORMING process. It consists of building the filament to the final specifications in terms of working current/voltage by using a dielectric breakdown process, i.e., an electric field is applied to the insulating oxide inducing O^{q-} species that drift towards the positively biased electrode, leaving behind charged O-deficient sites, referred to as oxygen vacancies (V_O in simplified Kröger–Vink notation).[9,17] The O-deficient filament makes an electrical contact between top electrode (TE) and bottom electrode (BE) (Figure 1(a)). In the case of properly designed stack, the FORMING step can be electrically similar to a SET process.[4,19] Furthermore, memory operation is based on the change in resistance in the weakest part of the filament that bottlenecks the current flow, i.e., the filament constriction. The location where the filament constriction grows during SET and shrinks during RESET is referred to as Switching Layer (SL). TE is the device region that provides with defects (vacancies/stores O atoms), referred hereafter as the Oxygen Exchange Layer (OEL, Figures 1(b)–1(d)), which acts as a defect reservoir or an active electrode. The last important constituent part of a RRAM device is the BE interface, which should have requirements on its own.

a)clima@imec.be

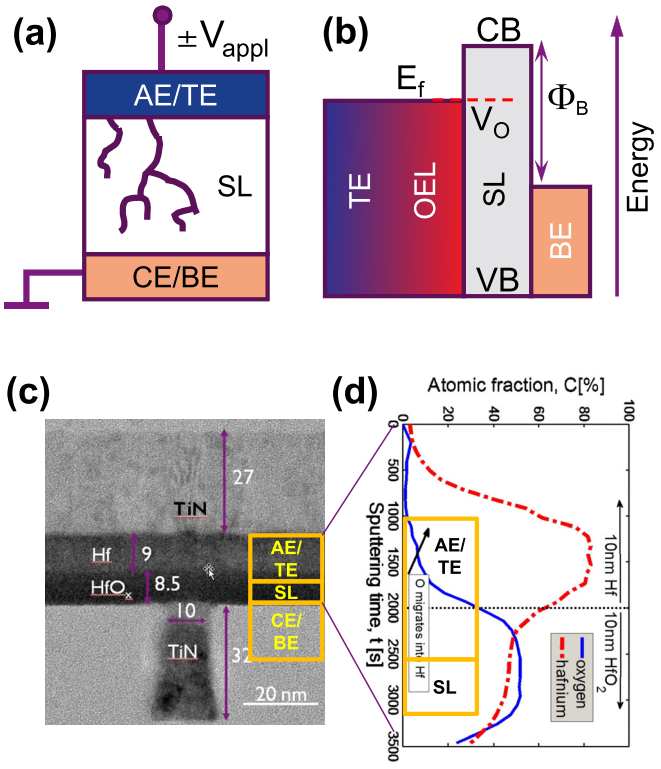

FIG. 1. (a) Schematic illustrations of filamentary RRAM device. Active electrode (AE) is the top electrode (TE) on which the voltage is applied. Counter electrode (CE) is the bottom electrode (BE) and the filament forms in the insulating switching layer (SL). (b) Electronic potential energy profile of a OxRAM stack—V_O filament in contact/equilibrium with Fermi level of the active electrode. VB/CB are the valence/conduction bands of the SL. (c) TEM picture of a typical Hf/HfO_x RRAM device (d) SIMS profile shows the O migration into scavenging layer.

The paper is structured as follows: Sections I and II set the general background, the motivation of the present analysis, and the methodology used. The body of the discussion is concentrated in Section III. It reviews the requirements to develop an efficient *active electrode*. The concept is illustrated on Hf,Ti and Ta top electrode materials. The identification of the best-performing properties of the *switching layer* is then discussed and illustrated on pure and Ti-, Si-, Al-doped oxides. The sought properties for the *counter-electrode* interface are then illustrated for the cases of TiN and Ru bottom electrode materials. We then conclude in Section IV of the paper.

II. METHODS AND MATERIALS

A. Test structures

Cross-point RRAM devices are integrated in a 1T1R CMOS compatible process scheme.[4] Atomic Layer Deposition (ALD) deposited amorphous oxide layers (HfOx, TaOx, HfAlOx) were sandwiched between TiN or Ru bottom electrode (BE) and PVD scavenging metals (Hf, Ti, Ta) with TiN on top electrode (TE). Devices down to 40 nm × 40 nm were processed.

B. Computational details

Density Functional Theory (DFT) is considered as the tool of choice when it comes to evaluate the thermodynamics of defect formation, driving forces for reactions in solid state materials, or the magnitude of kinetic barriers for those processes.[20,21] With the present account, we report defect formation energies, Nudged Elastic Band (NEB) kinetic barriers for atomic diffusion computed at the generalized gradient approximation (GGA) level, using the Perdew–Burke–Ernzerhof (PBE) exchange correlation functional[22] in combination with ultrasoft pseudopotentials.[23] The planewave expansion has been truncated at kinetic energies of 36 Ry and the integration of the Brillouin zone is usually done with a k-point mesh that has a density close to 20 points per $Å^{-1}$.[24] The generation of amorphous models has been performed with a classical molecular dynamics (MD) melt-and-quench technique followed by DFT relaxation. Accelerated MD was used to compute the diffusion coefficients.[25]

III. OxRAM STACK STRUCTURE

A. Active (top) electrode

1. Defect capacity

In the best-performing RRAM, the active electrode should be a **Defect reservoir** that provides unlimited conductive species to build up a filament. In this section, we analyze the thermodynamic driving factors to form such a defect reservoir. Before going into details, it is essential to establish the nature of the defects active in the switching process. For oxide-based RRAM (OxRAM), the conductive defects are the transition metal d orbitals that are not properly coordinated with O (called oxygen vacancy—V_O). They appear as a consequence of O^{q-} drift under the applied electric field. The O^{q-} species need to be temporarily stored (until next RESET cycle to rupture the filament) in a volume of material which should not change its metallic conductor character upon slight oxidation. For this reason, the defect reservoir in OxRAM is also called an Oxygen Exchange Layer. Small feature-size devices will require conformal deposition techniques like Atomic Layer Deposition (ALD). As a result, the films are deposited in conditions close to the thermodynamic equilibrium and therefore close to the stoichiometric composition. This is due to the highly exothermic oxide formation reactions.[26] The V_O^0 defect formation energy in stoichiometric oxides depends on the μ_O-oxygen chemical potential.[27] For amorphous models of HfO_2 and Ta_2O_5 (Figure 2(a)), we report the complete distribution of V_O formation energies in oxygen-rich condition in Figure 2(b), spreading from 3.8 to 5.8 eV in the case of HfO_2, and from −0.3 to 2.4 eV in the case of Ta_2O_5, depending on the local coordination of the O sites. The enthalpy of formation suggests that V_O form more easily in Ta_2O_5 than in HfO_2.

The defect formation energy defines its equilibrium concentration $c \sim N_{sites}\exp(-E_{form}/k_BT)$, where N_{sites} is the number of possible sites, E_{form} is the defect formation energy, k_B—Boltzmann constant, and T—absolute temperature.[28] The oxide in contact with O_2 is expected to contain a very low concentration of vacancy defects. The μ_O decreases by as much as 5.7[29]−5.8 eV at the oxygen-poor HfO_2-Hf interface (Figures 1(c) and 1(d)).[30] This shifts the V_O^0 formation energy distribution into exothermic region and increases exponentially the defect equilibrium concentration.[31] This results in the

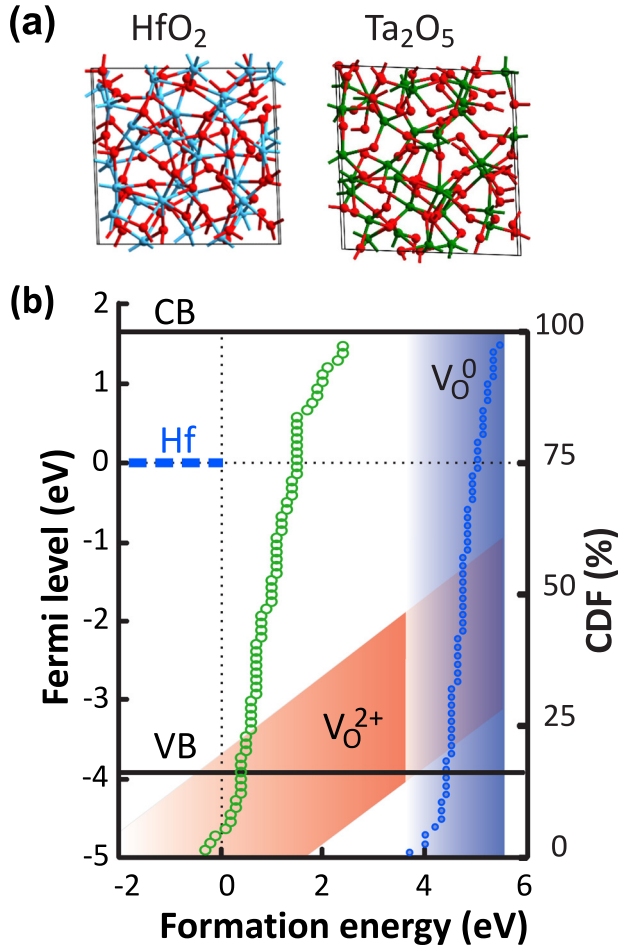

FIG. 2. (a) Atomic models of am-HfO_2 (Hf- blue, O-red) and am-Ta_2O_5 used to compute (b) the V_O (neutral—blue in HfO_2 and green in Ta_2O_5, shown for all vacancies as cumulative distribution function (CDF), 2+—red area for HfO_2 only) formation energy in O-rich conditions, as a function of electronic chemical potential—Fermi level, which in this case is aligned to the Hf metal.

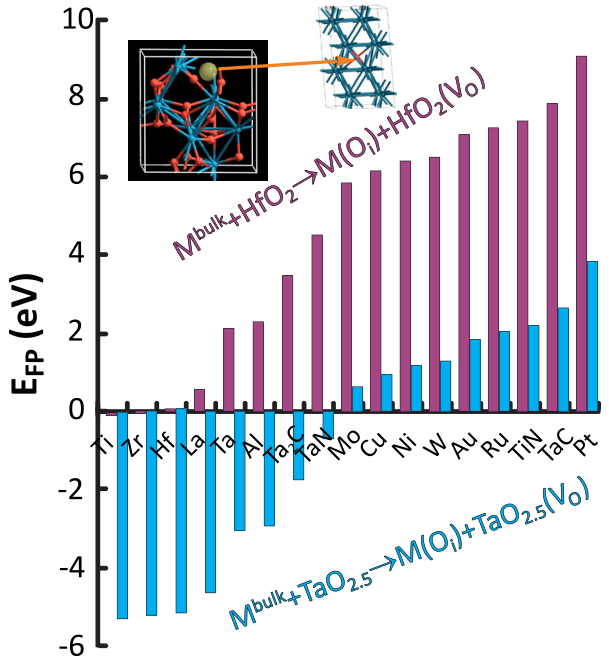

FIG. 3. Extended V_O-O_i Frenkel pair formation energy illustrating the different metal scavenging powers on HfO_2 and Ta_2O_5. Inset: O atoms become interstitial in the bulk metal to leave behind a vacancy.

generation of thermodynamic driving force that favors during the metal deposition on top of the switching oxide (in O-poor conditions) the creation of a large concentration of V_O in the oxide itself.[32] For that reason, the first capping metal layer on a ALD deposited oxide should be an oxygen-scavenging layer with the purpose to thin down the electrically insulating oxide switching layer thickness and to form a conducting sub-stoichiometric oxide, i.e., the oxygen exchange layer (Figures 1(b)–1(d)).

In fact, the reaction energetics depend on the nature of the scavenging metal in contact with the switching oxide.[33] In Figure 3, we show the energetics of the O transfer from an oxide to bulk metal as interstitial atom. In this particular example, we used HfO_2 and Ta_2O_5, for other oxides there is a rigid shift, corresponding to the difference in V_O formation energies. The lowest enthalpy of reaction results in a higher metal reactivity, therefore inducing a better O scavenging. The presented energetics are the sum of enthalpy of reaction computed for the formation of oxide V_O (endothermic for most systems) and metal oxide formation (exothermic for most oxides).

For this reason, the best scavenging effect is achieved with the use of a capping metal that can energetically compensate the O extraction process with the newly formed metal-oxygen bonds—for HfO_2 these are Hf, Zr, Ti. For Ta_2O_5, the vacancy formation energy is lower than for HfO_2; therefore, there are even more elements that can scavenge O atoms, such as La, Ta, Al.

The metal reactivity towards oxidation is inversely proportional to the metal workfunction—the more reactive metals have lower workfunction.[26] Experimentally, the deposited Hf capping using different thicknesses (Figure 4) suggests that capping layer thickness (longer reaction times) effectively thins down the switching layer which results in larger set/forming electric fields in the switching layer (Figure 4(b)). Therefore, the probability for a successful forming increases and the required voltages decrease, since the defect generation rate is field-accelerated, as approximated by the Arrhenius expression: $G = G_0 \exp[-(E_a - bF)/k_BT]$, where E_a is the activation energy of defect formation, b is the bond polarization factor, and F is the electric field.[34] The scavenging effect is further confirmed by the fact that higher energetics for O intake using, for instance, a Ta capping layer, results in a higher forming voltage if Ta is used as O scavenging metal.[35]

2. Defect mobility

Kinetic barriers for defect mobility are the critical aspect that defines the resistance switching dynamics and energy needs for the switching. Here, we analyze that aspect in the active electrode/oxygen exchange layer.

In analogy to the electrons and its complementary particles (holes), different mobility for the oxygen atoms and V_O can occur. In HfOx, the O diffusion coefficients are found to be rather similar in stoichiometric (switching layer) and sub-stoichiometric amorphous oxides (oxygen exchange layer) and are faster diffusing species than Hf atoms.[25]

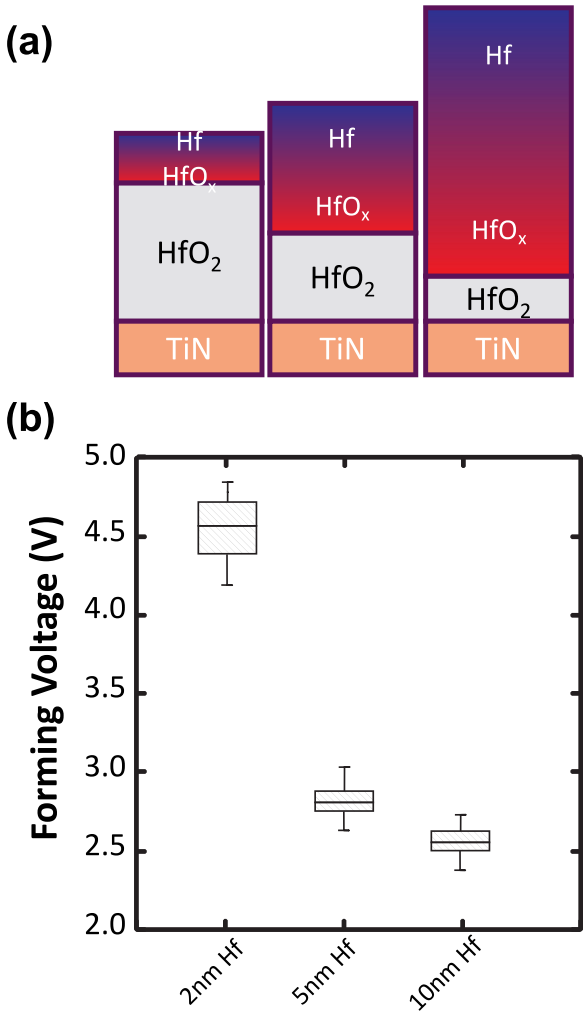

FIG. 4. Scavenging effect of metal capping layer—(a) proposed evolution of layer thickness with scavenging metal thickness, (b) forming voltage on 25 cells for 2/5/10 nm Hf capping thickness. The deposited HfO_2 thickness was 5 nm in 35 × 65 nm 0T1R.

These results indicate that the O drift-diffusion kinetic barriers define the global switching kinetics of HfO_2 switching layer. In pure metals, the diffusion barriers of interstitial O can vary in a wide range (0.9 eV in Ta, 2.5 eV in Hf, Figure 5(a)) Hence, inter-mixing is important not only for low thermodynamic driving force of the oxygen exchange layer but also helps reducing the kinetic barriers. The latter do not need to be too high, in order to prevent the shortage in defect supply from oxygen exchange layer.

For HfO_x-based RRAM devices, we can conclude that the sub-stoichiometric layer plays the role of oxygen exchange layer, not the pure metal. This is consistent with the findings reported for the explicit crystalline Hf/HfO_2 interface calculations.[36]

3. Defect stability

The LRS state of the OxRAM constitutes an unstable state of the system that has a thermodynamic driving force to be stabilized towards the fully oxidized filament (Figure 6(a)). For a single V_O, ΔG can be approximated to the Frenkel pair formation energy reported in Figure 3. From this point of view, it is important that the potential energy of the O (its chemical potential) in the oxygen exchange layer/active electrode is low enough to have the lowest thermodynamic driving force possible. To illustrate the issue, we consider the case of Hf and Ta scavenger layers acting on HfO_2. In the theoretical limiting case of a perfect bulk metal/oxide interface (TE/switching layer Figure 5(b)), interstitial O in Ta layer has ∼2 eV higher potential energy than in Hf (therefore larger thermodynamic driving force) to leave the interstitial position and oxidize the filament in switching layer. For the intermixing interface (oxygen exchange layer/switching layer Figure 5(c)), we can consider in a first approximation that the chemical potential lies in-between the two neighboring layers. Together with the computed kinetic barriers (Figure 5(a)), we can predict that in the long-term the filament has higher probability to oxidize faster with Ta cap than with the Hf cap. As an experimental confirmation, the faster retention failure of a RRAM device with Ta cap, compared to the one with Hf cap (Figure 6(b)) points towards this effect.

Set in a general perspective, these findings suggest that each metal/oxide stack has its own chemical potential profile and kinetic barriers that defines the thermodynamic driving force of the O biased-diffusion towards a particular layer and the rates at which it occurs. In order to design the best-performing RRAM device, the oxygen exchange layer energetic profile needs to show low ΔG thermodynamic driving force and the diffusion kinetics to be comparable to the switching layer defect mobility.

B. Switching layer

1. Filament stability

Because of the abundance of defects in oxygen exchange layer (being largely sub-stoichiometric), the switching layer

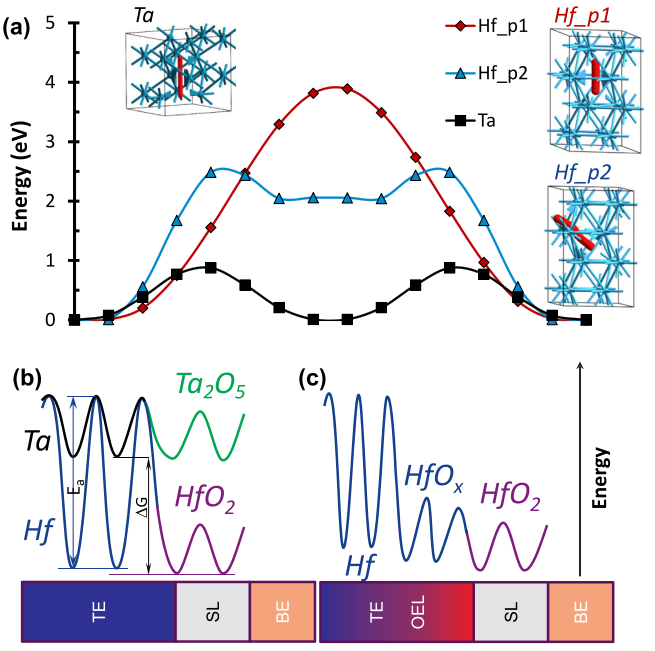

FIG. 5. (a) NEB paths for O_i diffusion in bulk Hf/Ta metals. (b) Qualitative potential energy surface diagram for oxygen atoms in unmixed metal/oxide interface and (c) in the inter-mixed interface (for Hf/HfO_x/HfO_2 interface).

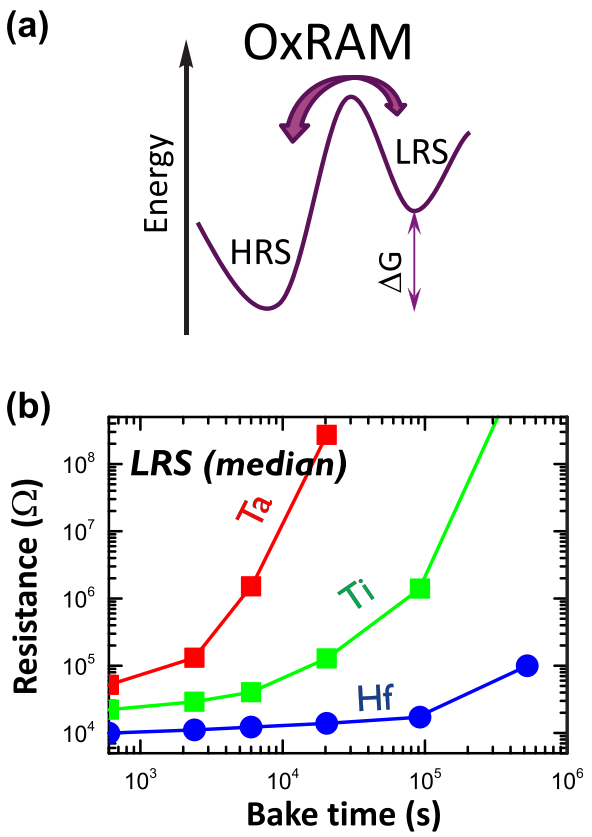

FIG. 6. (a) Low Resistance State (LRS) is the energetically meta-stable state of the system that tends towards the more stable High Resistance State (HRS). (b) Hf scavenging layer shows longer retention of the LRS state (median value of >100 devices across the wafer).

acts as a constriction/bottleneck for the current in the filament. In other words, the filament constriction is always located in the switching layer. Whatever the thermodynamic spontaneity/driving force of a particular filament, its retention (stability in time) is defined by the kinetic barriers encountered by the O atoms that need to diffuse. The disorder in the grain boundaries or amorphous materials (typical location of filaments in OxRAM) introduces a wide distribution of those kinetic barriers.[29] That is, in contrast to the perfect crystalline bulk that shows a limited number of kinetic barrier heights.[37] To that end, the NEB kinetic barriers of next-neighbor O-V_O exchange have been computed for amorphous HfO_2 and Ta_2O_5 models.[29] It is reported that large distribution of barrier heights of up to 4–5 eV is present in the both systems. Of course during the filament retention, the lowest barriers allow the defect to change faster its energetic landscape and position. If present in the filament critical path, those defects produce fast-decaying resistance distribution tails, therefore presenting reliability issues. Kinetic barriers below 0.8–0.9 eV give early filament LRS failure. Given that the spatial distribution of the kinetic barriers is non-uniform, agglomerations of high kinetic barriers and of low kinetic ones even in amorphous state materials can be observed.[38] The spread in kinetic barrier heights and the dynamic heterogeneities has been reported to be the main source of intrinsic variability (retention, switching parameters, endurance) of filamentary/amorphous—based RRAM devices.[29]

The desirable kinetic barrier height window for the switching layer is to be located between 0.8–1.6 eV. Smaller values would lead to a short retention, whereas larger ones would lead to harder-to-switch pool of defects that would consume too much energy per switching event, which is opposed to lower switching energy, desirable in most of the RRAM applications.[4] Note that a factor that is not considered in this work is the defect clustering and its impact on the filament stability.[39]

2. Switching process

By moving the O atoms in/out of the constriction, there can be less/more current-defining defects, which can result in RESET/SET of the device (switching it OFF/ON). The switching dynamics (time, but also voltage, current, energy) are therefore defined by the O drift under applied electric field during the switching operations. During the SET process, the electric field exerts both a barrier-lowering effect on the aforementioned kinetic barriers,[40] and an energy-stabilization effect of the charged defects (Figure 2(b)). The barrier-lowering effect is only 3%–30% in OxRAM.[41] On top of that, there is a change of kinetic barrier height (E_a) when the defects are positively charged.[29] The best-performing materials should have the field-enhanced drift as

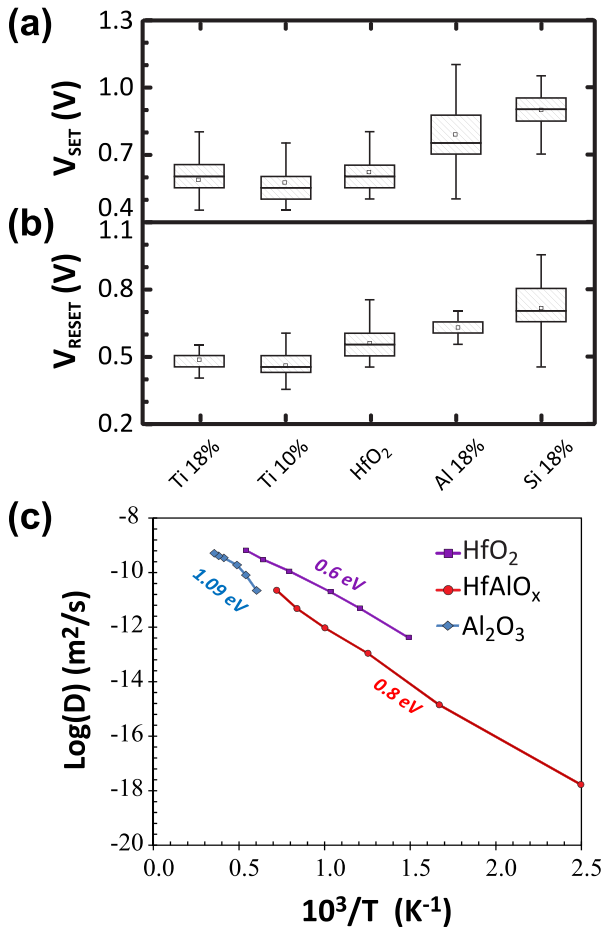

FIG. 7. (a) SET and (b) RESET voltage distributions in Ti-, Al-, and Si-doped HfO_2 switching layers. (c) Accelerated MD simulations of O diffusion in a single amorphous sample (qualitative insight) of alumina, hafnia, and hafnium aluminate.

high as possible to decrease the switching time, while keeping a long retention at rest. The RESET process is more complex. As a first order approximation, a complete filament can be described as a quantum-point-contact. The difficulty is to initiate the filament dissolution in the absence of a field enhancement.

Therefore, a certain Joule heating process is required to provide enough kinetic energy to the defects from the constriction to disperse and for the electric field to appear, inducing a field-enhanced drift process (in the reverse direction, compared to SET). Since in OxRAM the workfunctions of the two electrodes are different by the definition of the stack (low workfunction for TE to be O-reactive and form oxygen exchange layer and high BE workfunction for a O-inert BE as discussed in the next paragraph), generally the needed RESET voltage should be lower, compared to the SET one (Figures 7(a) and 7(b)).

3. Defect drift-diffusion barrier tuning

Given that the need for a specific window for kinetic barriers has been established, we now need to be able to tune them. At the atomic scale, the barrier heights tunability is reduced ultimately to the strength of the bond with the oxygen atoms. Therefore doping the OxRAM switching layer material with either Al or Si (two of the strongest O-bond forming elements) should have a retarding effect on O diffusion, as qualitatively described by accelerated MD simulations of O diffusion in amorphous models of HfO_2, Al_2O_3, and $HfAlO_x$ models in Figure 7(c)—$HfAlO_x$ shows consistently lower diffusion coefficients than HfO_2 does at any considered temperature, also the slope (Arrhenius activation energy) is ~0.2 eV larger. As an experimental verification, we present the switching voltage distributions for Ti-, Al-, and Si-doped HfO_2 switching layer devices (with the rest of the stack identical) in Figures 7(a) and 7(b). Ti doping leads to somewhat lower switching voltages compared to pure HfO_2, whereas Al and Si dopings require consistently larger switching voltages.

C. Counter (bottom) electrode

1. Electronic and ionic potential barriers

In contrast to the electronic (Figure 1(b)) and ionic (for O atoms, Figures 5(b) and 5(c)) potential energy landscape for TE(oxygen exchange layer)/switching layer interface, which should be neither an electronic barrier nor a O barrier, the switching layer/BE interface must behave as blocking interface for both electrons and defects/O ions. Otherwise, the RRAM device can change the bipolar behavior to a complementary switching.[42] Whatever the type of the defects in the RRAM device, they are generally accompanied by a certain electronic flux flowing in the opposite drift direction of the active defects during the switching. On top of the displacement current, there should be a certain electric current in the external circuit, required to sustain the redox processes of the defects. The former is present only during the SET operation and can be made negligible with nano-sized electrodes and moderate dielectric constant switching layer. The internal leakage has hence to be reduced to the absolute minimum for low-current applications. For that reason, a high workfunction BE is necessary. This guarantees that the electrons encounter a high Schottky barrier height during the SET process (see Figure 1(b) for the electronic potential energy surface).

In addition to electronic barrier properties discussed above, the switching layer/BE interface has also to prevent the O atoms from leaving the switching layer (Figure 8(a)). To illustrate the point, we compare the cases of TiN and Ru as BE. Ideal interstitial oxygen (O_i) in TiN leads to a rather high energy situation (Figure 3). This picture can change dramatically towards a more stable oxygen on nitrogen

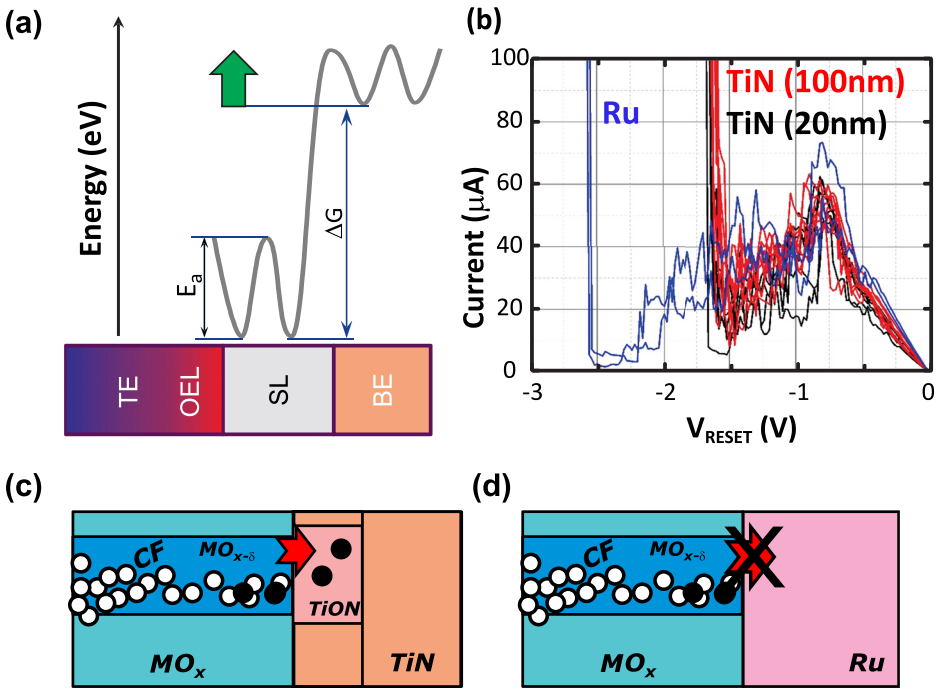

FIG. 8. (a) Illustration of the O atoms potential energy surface expected at the switching layer/BE interface. (b) Experimental comparison of DC RESET breakdown in devices with TiN and Ru as BE.[43] ((c) and(d)) Atomic model that we propose to explain the evidenced device degradation.

position (O_N) when nitrogen vacancy (V_N) sites are available.[44] In Table I, we report the barrier height for the O_N migration (TiON) to be 3 time higher compared to O_i in TiN. Same energetic advantage is present in grain boundaries, which can easily accommodate O atoms bonded to Ti atoms because of the formation of highly exothermic Ti-O bonds. Ru oxidation, on the other hand, is intrinsically much less exothermic than Ti,[26] therefore providing a better O barrier. As an experimental confirmation of this scheme, we measure RESET breakdown of a TaOx stack with TiN and Ru BE (Figure 8(b)).[43] During RESET, a negative voltage is applied on the TE. The resulting electric current dissolves/forms the constriction (first peak at ~0.5−0.75 V Figure 8(b)), afterwards drive O^{q-} from oxygen exchange layer into switching layer, increasing the constriction. If the BE interface is not a good barrier for the O^{q-} species (due to some issues with TiN grain boundaries, V_N,…), the O^{q-} species could penetrate into BE as well at excessive applied energy (Figure 8(c)). In that case V_O defects are left behind: filament forms from the wrong side of the device, cancelling the asymmetry of the RRAM. As seen in Figures 8(b) and 8(d), the Ru BE can withstand higher electric fields (up to 2.6 V) without breaking down, compared to TiN (up to 1.7 V) at which point, most of the devices fail shorted.

The same process can take place gradually in the course of device operation the generation of extra defects, showing a resistance degradation during the device endurance. Experimentally, the effect can be accelerated with an unbalanced (stronger) RESET voltage, as shown in Figures 9(b) and 9(c). The Ru BE is more robust and can withstand more programing cycles than TiN BE (Figure 9(d)) even at a more aggressive reset voltage.[43] The proposed atomic model is depicted in Figure 8(c)—constantly forcing an over-RESET voltage drives irreversibly O atoms into BE, therefore lowering the filament resistance. The upside of switching layer/BE interface energetics is that the high workfunction metals do not compromise the O defect barrier—higher workfunction/Schottky barrier height is directly (inversely) proportional to the O barrier (scavenging power) of the electrode.[26]

2. Defect kinetics and thermodynamic in BE materials

We have qualitatively established that the BE needs to be an ionic/electronic barrier in Sec. III C 1. The BE oxidation being a highly endothermic process it is in itself a good barrier against the oxidation of Ru, even if O_i diffusion kinetic barriers in bulk Ru are modest (1–2 eV, Table I). In the case of a crystalline TaN phase, the required oxidation free energy is lower, but in combination with rather large internal diffusion kinetic barriers, TaN still can resist further oxidation.

TABLE I. O diffusion kinetic barriers (E_a) in several BE materials (NEB calculated and literature data) and thermodynamic endothermicity (ΔE) of O transfer from HfO_2 and Ta_2O_5 oxides to the metal electrode materials.

BE	Exp E_a (eV)	Calc E_a (eV)	$\Delta E(HfO_2)$ (eV)	$\Delta E(Ta_2O_5)$ (eV)
Hf	1.7–2.2	2.5	~0	−5.2
Ta	1.2	0.9	2.2	~−3.0
Ru	1.0–1.3[5]	1.5–2.0	7.2	2.0
TiN	2.0[4],1.7[6]	0.9	7.4	2.2
TiON	…	2.6	~1	…
TaN	…	5-7	~4.5	−0.7

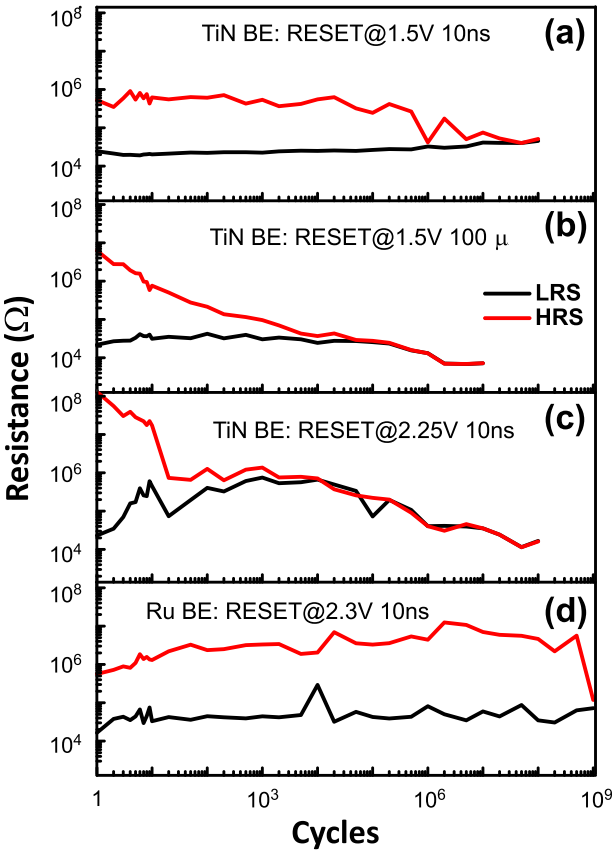

FIG. 9. (a) Endurance degradation in Ta/TaOx/BE can be accelerated with (b) prolonged pulse time (100 μs) or (c) an increasingly higher RESET voltage (2.25 V). (d) Endurance with Ru BE at 2.3 V.[43]

IV. CONCLUSIONS

To ensure excellent cyclability and retention, the RRAM cell has to have a good defect reservoir that is asymmetrically located on one side of the device. This can be achieved with an oxygen scavenging metal (chosen among the easily oxidizable metal) layer in contact with the switching oxide. Thin switching layer can lead to forming-free operation of RRAM. The kinetic barriers for the O diffusion define the switching speed, energy, and retention. In amorphous materials, there is a distribution of kinetic barriers that leads to the evolution of resistance statistical tails. The nature of the bottom electrode material has to play the role of an ionic/electronic barrier. It has to display a high workfunction and be inert with respect to the oxidation. Therefore, RRAM stack asymmetry in terms of defect concentration and ionic/electronic barriers is the key ingredient to ensure a reliable longevity of the RRAM memory cell (endurance and retention).

ACKNOWLEDGMENTS

This work was carried out in the framework of the imec Core CMOS—Emerging Memory Program.

[1]L. Seung Ryul, K. Young-Bae, C. Man, K. Kyung Min, L. Chang Bum, H. Ji Hyun, P. Gyeong-Su, L. Dongsoo, L. Myoung-Jae, K. Chang Jung, U. I. Chung, Y. In-Kyeong, and K. Kinam, in Proceedings of the IEEE Symposium on VLSI Technology, 2012, pp. 71–72.

[2]B. Govoreanu, S. Kubicek, G. Kar, Y.-Y. Chen, V. Paraschiv, M. Rakowski, R. Degraeve, L. Goux, S. Clima, N. Jossart, C. Adelmann, O. Richard, T. Raes, D. Vangoidsenhoven, T. Vandeweyer, H. Tielens, K. Kellens, K. Devriendt, N. Heylen, S. Brus, B. Verbrugge, L. Pantisano, H. Bender, G. Pourtois, J. A. Kittl, D. J. Wouters, L. Altimime, and M. Jurczak, Extended Abstracts on SSDM Conference, Nagoya, Japan, 2011, pp. 1005–1006.

[3]Y. S. Chen, H. Y. Lee, P. S. Chen, C. H. Tsai, P. Y. Gu, T. Y. Wu, K. H. Tsai, S. S. Sheu, W. P. Lin, C. H. Lin, P. F. Chiu, W. S. Chen, F. T. Chen, C. Lien, and M. J. Tsai, IEEE Int. Electron Devices Meet. 31.33.31–31.33.34 (2011).

[4]B. Govoreanu, G. S. Kar, Y. Chen, V. Paraschiv, S. Kubicek, A. Fantini, I. P. Radu, L. Goux, S. Clima, R. Degraeve, N. Jossart, O. Richard, T. Vandeweyer, K. Seo, P. Hendrickx, G. Pourtois, H. Bender, L. Altimime, D. J. Wouters, J. A. Kittl, and M. Jurczak, IEEE Int. Electron Devices Meet. 31.36.31–31.36.34 (2011).

[5]A. Fantini, L. Goux, S. Clima, R. Degraeve, A. Redolfi, C. Adelmann, G. Polimeni, Y. Y. Chen, M. Komura, A. Belmonte, D. J. Wouters, and M. Jurczak, in Proceedings of the IEEE 6th International Memory Workshop (IMW), 2014, pp. 1–4.

[6]K. M. Kim, D. S. Jeong, and C. S. Hwang, Nanotechnology **22**(25), 17 (2011).

[7]S. Clima, K. Sankaran, Y. Y. Chen, A. Fantini, U. Celano, A. Belmonte, L. Zhang, L. Goux, B. Govoreanu, R. Degraeve, D. J. Wouters, M. Jurczak, W. Vandervorst, S. De Gendt, and G. Pourtois, Phys. Status Solidi-Rapid Res. Lett. **8**(6), 501–511 (2014).

[8]Y. C. Yang, P. Gao, L. Z. Li, X. Q. Pan, S. Tappertzhofen, S. Choi, R. Waser, I. Valov, and W. D. Lu, Nat. Commun. **5**, 4232 (2014).

[9]R. Waser, R. Dittmann, G. Staikov, and K. Szot, Adv. Mater. **21**(25–26), 2632–2663 (2009).

[10]D. Ielmini and R. Waser, *Resistive Switching: From Fundamentals of Nanoionic Redox Processes to Memristive Device Applications* (Wiley, 2016).

[11]J. J. Yang, D. B. Strukov, and D. R. Stewart, Nat. Nanotechnol. **8**(1), 13–24 (2013).

[12]D. S. Jeong, H. W. Schroeder, and R. Waser, Phys. Rev. **79**(19), 195317 (2009).

[13]D. Ielmini, S. Spiga, F. Nardi, C. Cagli, A. Lamperti, E. Cianci, and M. Fanciulli, J. Appl. Phys. **109**(3), 034506 (2011).

[14]Y. S. Lin, F. Zeng, S. G. Tang, H. Y. Liu, C. Chen, S. Gao, Y. G. Wang, and F. Pan, J. Appl. Phys. **113**(6), 064510 (2013).

[15]Z. Hiroi, Prog. Solid State Chem. **43**(1–2), 47–69 (2015).

[16]B. Govoreanu, A. Redolfi, L. Zhang, C. Adelmann, M. Popovici, S. Clima, H. Hody, V. Paraschiv, I. P. Radu, A. Franquet, J.-C. Liu, J. Swerts, O. Richard, H. Bender, L. Altimime, and M. Jurczak, IEEE Int. Electron Devices Meet. **10**(12), 14 (2013).

[17]R. Waser, R. Dittmann, M. Salinga, and M. Wuttig, Solid-State Electron. **54**(9), 830–840 (2010).

[18]M. J. Rozenberg, M. J. Sanchez, R. Weht, C. Acha, F. Gomez-Marlasca, and P. Levy, Phys. Rev. B **81**(11), 115101 (2010).

[19]S. U. Sharath, T. Bertaud, J. Kurian, E. Hildebrandt, C. Walczyk, P. Calka, P. Zaumseil, M. Sowinska, D. Walczyk, A. Gloskovskii, T. Schroeder, and L. Alff, Appl. Phys. Lett. **104**(6), 063502 (2014).

[20]C. G. Van de Walle and A. Janotti, in *Advanced Calculations for Defects in Materials* (Wiley-VCH Verlag GmbH and Co. KGaA, 2011), pp. 1–16.

[21]G. Henkelman, B. P. Uberuaga, and H. Jonsson, J. Chem. Phys. **113**(22), 9901–9904 (2000).

[22]J. P. Perdew, M. Emzerhof, and K. Burke, J. Chem. Phys. **105**(22), 9982–9985 (1996).

[23]D. Vanderbilt, Phys. Rev. B **41**(11), 7892–7895 (1990).

[24]P. Giannozzi, S. Baroni, N. Bonini, M. Calandra, R. Car, C. Cavazzoni, D. Ceresoli, G. L. Chiarotti, M. Cococcioni, I. Dabo, A. Dal Corso, S. de Gironcoli, S. Fabris, G. Fratesi, R. Gebauer, U. Gerstmann, C. Gougoussis, A. Kokalj, M. Lazzeri, L. Martin-Samos, N. Marzari, F. Mauri, R. Mazzarello, S. Paolini, A. Pasquarello, L. Paulatto, C. Sbraccia, S. Scandolo, G. Sclauzero, A. P. Seitsonen, A. Smogunov, P. Umari, and R. M. Wentzcovitch, J. Phys.-Condens. Matter **21**(39), 395502 (2009).

[25]S. Clima, Y. Y. Chen, R. Degraeve, M. Mees, K. Sankaran, B. Govoreanu, M. Jurczak, S. De Gendt, and G. Pourtois, Appl. Phys. Lett. **100**(13), 133102 (2012).

[26]O. Sharia, K. Tse, J. Robertson, and A. A. Demkov, Phys. Rev. B **79**(12), 125305 (2009).

[27]J. L. Lyons, A. Janotti, and C. G. Van de Walle, Microelectron. Eng. **88**(7), 1452–1456 (2011).

[28]C. G. Van de Walle and A. Janotti, Phys. Status Solidi B **248**(1), 19–27 (2011).

[29]S. Clima, Y. Chen, A. Fantini, L. Goux, R. Degraeve, B. Govoreanu, G. Pourtois, and M. Jurczak, IEEE Electron Device Lett. **36**(8), 769–771 (2015).

[30]K. Y. Tse, D. Liu, and J. Robertson, Phys. Rev. B **81**(3), 035325 (2010).

[31]Y. Guo and J. Robertson, Microelectron. Eng. **147**, 339–343 (2015).

[32]S. Clima, B. Govoreanu, M. Jurczak, and G. Pourtois, Microelectron. Eng. **120**, 13–18 (2014).

[33]N. Zhong, H. Shima, and H. Akinaga, Appl. Phys. Lett. **96**(4), 042107 (2010).

[34]G. Bersuker, D. C. Gilmer, D. Veksler, P. Kirsch, L. Vandelli, A. Padovani, L. Larcher, K. McKenna, A. Shluger, V. Iglesias, M. Porti, and M. Nafria, J. Appl. Phys. **110**(12), 124518 (2011).

[35]L. Goux, A. Fantini, A. Redolfi, C. Y. Chen, F. F. Shi, R. Degraeve, Y. Y. Chen, T. Witters, G. Groeseneken, and M. Jurczak, in Proceedings of the Symposium on VLSI Technology, 2014, pp. 1–2.

[36]A. O'Hara, G. Bersuker, and A. A. Demkov, J. Appl. Phys. **115**(18), 183703 (2014).

[37]A. S. Foster, A. L. Shluger, and R. M. Nieminen, Phys. Rev. Lett. **89**(22), 225901 (2002).

[38]D. Chandler and J. P. Garrahan, Annu. Rev. Phys. Chem. **61**, 191–217 (2010).

[39]K. Kamiya, M. Y. Yang, S.-G. Park, B. Magyari-Koepe, Y. Nishi, M. Niwa, and K. Shiraishi, Appl. Phys. Lett. **100**(7), 073502 (2012).

[40]G. Bersuker, B. Butcher, D. Gilmer, P. Kirsch, L. Larcher, and A. Padovani, in Proceedings of the 43rd European Solid-State Device Research Conference, 2013, pp. 163–165.

[41]R. Degraeve, A. Fantini, N. Raghavan, Y. Y. Chen, L. Goux, S. Clima, S. Cosemans, B. Govoreanu, D. J. Wouters, P. Roussel, G. S. Kar, G. Groeseneken, and M. Jurczak, in Proceedings of the Symposium on VLSI Technology, 2013, pp. T98–T99.

[42]A. Schonhals, D. Wouters, A. Marchewka, T. Breuer, K. Skaja, V. Rana, S. Menzel, and R. Waser, in Proceedings of the IEEE International Memory Workshop (IMW), 2015, pp. 1–4.

[43]C. Y. Chen, L. Goux, A. Fantini, A. Redolfi, S. Clima, R. Degraeve, Y. Y. Chen, G. Groeseneken, and M. Jurczak, IEEE Int. Electron Devices Meet. **14**(12), 14.2.1–14.2.4 (2014).

[44]S. R. Bradley, K. P. McKenna, and A. L. Shluger, Microelectron. Eng. **109**, 346–350 (2013).